JOURNAL GEOLOGICAL SOCIETY OF INDIA
Vol.79, February 2012, pp.199-209

Geothermal Modeling for the Base of Gas Hydrate Stability Zone and Saturation of Gas Hydrate in the Krishna-Godavari Basin, Eastern Indian Margin

Uma Shankar[1], Kalachand Sain[1] and Michael Riedel[2]
[1]CSIR-National Geophysical Research Institute, Uppal Road, Hyderabad - 500 007
[2]Natural Resources Canada, Pacific Geoscience Center, Geological Survey of Canada,
9860 W. Saanich Rd. Sidney, B.C. V8L 4B2, Canada
Email: umashankar_ngri@yahoo.com, kalachandsain@yahoo.com; mriedel@nrcan.gc.ca

Abstract: The passive eastern Indian margin is rich in gas hydrates, as inferred from the wide-spread occurrences of bottom-simulating reflectors (BSRs) and recovery of gas hydrate samples from various sites in the Krishna Godavari (KG) and Mahanadi (MN) basins drilled by the Expedition 01 of the Indian National Gas Hydrate Program (NGHP). The BSRs are often interpreted to mark the thermally controlled base of gas hydrate stability zone (BGHSZ). Most of the BSRs exhibit moderate to typically higher amplitudes than those from other seismic reflectors. We estimate the average geothermal gradient of ~40^0C/km and heat flow varying from 23 to 62 mW/m^2 in the study area utilizing the BSR's observed on seismic sections. Further we provide the BGHSZ where the BSR is not continuous or disturbed by local tectonics or hidden by sedimentation patterns parallel to the seafloor with a view to understand the nature of BSR.

Since, gas hydrate bearing sediment has higher electrical resistivities than that of the host sediment, we estimate two levels of gas hydrates saturations up to 25% in the depth interval between 70 to 82, and less than 20% in the depth interval between 90 to 104 meter below the seafloor using the resistivity log data at site 15 of NGHP-01.

Keywords: Gas hydrates, Bottom simulating reflectors, Geothermal gradient, Resistivity log, Saturation, KG basin, Eastern Indian margin.

INTRODUCTION

Gas hydrates are crystalline form of mainly methane and water, and are found along the continental margins and permafrost regions where the pressure and temperature are favorable for gas hydrate stability (Kvenvolden, 1998). Gas hydrates are inferred from multi-channel seismic (MCS) data through the observations of bottom simulating reflections (BSRs), which can be identified based on characteristics of reverse polarity with respect to the seafloor reflection, cross-cutting dipping sedimentary reflections and parallel to the seafloor reflection on a regional scale (Shipley et al. 1979; Hyndman and Spence, 1992; Minshull et al. 1994). The BSR, coinciding with the base of gas hydrate stability zone (BGHSZ), is a disseminated boundary in marine sediment. Presence of gas hydrate reduces the permeability and hence trap free-gas underneath. Thus the BSR represents a physical boundary between the hydrate bearing sediments above and gas-bearing sediments below.

The high-resolution MCS surveys have been carried out for the exploration of gas hydrates in the Krishna-Godavari (KG) basin, off the eastern Indian margin. The widespread BSRs, observed on seismic sections, indicate potential occurrences of gas-hydrates in the KG basin (Bastia, 2006; Collett et al. 2008; Sain and Gupta, 2008; Ramana et al. 2009; Shankar and Riedel, 2010). The BSRs are heterogeneous in character and are limited to local areas even though the gas hydrate is stable under prevalent thermo baric conditions at water depths between 800 to 1500 m. Factors such as the bathymetry, temperature, origin and composition of gaseous hydrocarbons and geological structures favor the formation of gas hydrates in most parts of the KG basin (Sain and Gupta, 2008). However, the drilling and coring results show gas hydrates in massive lumps, and possibly in finely-distributed grain-displacing, fracture-fill, small nodules, or lenses (Collett et al. 2008).

The thickness of gas hydrate stability zone (GHSZ) varies widely within oceanic sediments by various parameters such as the ocean bottom water temperature, geothermal gradient, pressure (depth), salinity of formation water, and composition of gas (Sloan, 1990). The continental

margins show a shoaling of the BGHSZ, which often marks the region of slope instability, and gas venting through tectonic disturbances such as folding and faulting (Kvenvolden, 1999; Hovland et al. 2002).

Gas hydrates have also been reported without BSRs from different margins, particularly from areas of active fluid flow through the seafloor as evidenced by pockmarks, gas chimneys, and mud mounds (Holbrook et al., 1996; Sager et al. 1999, Riedel et al. 2006; Ramana, et al. 2006). Fluid flow is often related to active faulting that may affect gas hydrate stability conditions prevalent at that location (Fichler et al. 2005). Fluid flow along faults may induce variations in geothermal gradient also (Cooper and Hart, 2003; Ruppel et al. 2005). In such regions, the geometry of the BGHSZ could vary significantly (laterally) preventing the formation of any noticeable BSR. Here, we analyze and model the BGHSZ in the KG Basin (Fig. 1) using the MCS data, regional bathymetry, seafloor temperature and geothermal gradient from the NGHP-01 (Collett et al. 2008). We also estimate the geothermal gradient and heat flow from the subsurface depths of BSRs. Knowledge of heat-flow regime and the thickness of GHSZ provide important inputs to understand the petroleum system and to model the basin evolution. Additionally, knowledge of overall GHSZ is useful for global carbon-cycling models. The estimate of GHSZ is also important to assess the drilling-hazards as well as geo-hazards that may lead to slumping and slope-failure in an area.

The KG basin and other areas of the Indian continental margins are known for their large sediments influx from vast river system providing a large sediment load as well as organic carbon input into the deep sea environment. The KG basin is characterized by a zone of extensive toe-thrusts (Riedel et al. 2010), which significantly shape the seafloor morphology and can therefore affect the thermal regime and BGHSZ. If fluid-migration along such faults exists, the BGHSZ can be altered. Modeling the BGHSZ based on a purely conductive regime can therefore help assess the possible presence of fluid migration. This, in turn, provides implications on the overall fluid-circulation pattern of a basin.

The thermal structure along a margin is generally assessed from heat flow studies carried out on the seafloor. The heat flow can be calculated from the thermal conductivity of near-surface material and geothermal gradient. The conductivity at a location can be measured either in situ or from materials recovered by gravity or piston coring from the seafloor. The temperature gradient is derived from a set of in situ temperature measurements. However, the direct measurement of heat flow is a very slow procedure and provides information only at discrete locations. We estimate the geothermal gradients and heat flows at various locations from the depths of BSRs identified on seismic sections.

Presence of gas hydrates in the pore spaces of marine sediments can affect the bulk physical properties of the sediment. The measurement of such properties can therefore be used to estimate gas hydrate saturation. The well log and the MCS data can be used to understand the nature of distribution and quantification of gas hydrates and free gas within the sediments (Andreassen, 1995; Yuan et al., 1996; Sloan, 1998; Paull and Dillon, 2001). Natural gas hydrate formation reduces the effective porosity and electric conduction, so that gas hydrate bearing sediment has high electrical resistivity. Down-hole resistivity logs can thus be used for characterizing the in situ properties of gas hydrate bearing sediments and estimation of gas hydrates (Guerin et al. 1999; Helgerud et al. 1999; Hyndman et al. 2001; Collett, 2002; Lee and Waite, 2008).

Here we have estimated the gas hydrate saturation using the Archie's (1942) law from the electrical resistivity log data at site 15 of the NGHP-01 at water depth of ~926 m in the KG basin (Fig. 1). Unlike at site 10D, no large piece or massive of gas hydrates were recovered at this site, dispersed gas hydrates have been inferred at this location (Collett et al. 2008). So we assume that the gas hydrates have primarily replaced a portion of sediment pore fluids. The gas hydrate saturation versus resistivity may be different in the case of massive gas hydrates deposit (Mathews, 1986).

GEOLOGY AND TECTONIC SETTING OF KG BASIN

The eastern continental margin of India formed as a result of rifting between India and the rest of East Gondwanaland (Australia/Antarctica) in the Late Jurassic and Early Cretaceous (Ramana et al. 2001). Rifting began in the Late Jurassic at about 160 Ma with breakup at ~130 Ma (Powell et al. 1988). Sediment input to the Bay of Bengal in the eastern Indian Margin is dominated by the Ganges-Brahmaputra river system. The resulting sediment influx has built the Bengal Fan, the world's largest sediment accumulation. The sediment thickness of the Bengal Fan reaches a maximum of over 22 km on the Bangladesh shelf (Curray, 1991) and over 2 km of fan sediments are found at 2°S (Curray et al. 1982). The Late Jurassic rift structures along the eastern margin cut across older NW-SE trending Permian-Triassic Gondwana grabens including the Mahanadi and Pranhita-Godavari grabens (Sastri et al. 1981). The Mahanadi graben appears to have a continuation

in Antarctica that is the Lambert graben (Federov et al. 1982). These structures serve to delineate the fluvial drainage system throughout the evolution of the Indian margin to the present and they now contain the Mahanadi and Godavari Rivers. Both rivers have high sediment transport (Sastri et al. 1981; Biksham and Subrahmanyam, 1988) and built substantial deltas.

The KG Basin is located in a passive margin setting, and is known as a peri-cratonic rift basin (Rao, 2001). It is located on the central part of the eastern Indian margin (Fig. 1). The offshore basin including the delta region of Krishna and Godavari rivers covers an area of ~24000 km^2 up to isobaths of 200 m. The basin extends into deeper water and covers a much larger area of ~145000 km^2 (Ramana et al. 2009). The maximum sediment thickness in the KG Basin extends up to 8 km (Prabhakar and Zutshi, 1993; Rao, 2001). This stretch of sedimentary region contains a vast range of geologic settings, such as the costal basin, delta, shelf-slope apron, deep-sea channel, and deep-water fan complex. The basin is characterized with horst and graben systems, which are filled with thick sediments of Permian-to-Recent age and emerged as one of the frontier areas for future hydrocarbon exploration. Discovery of conventional gas and large deposit of gas hydrates in recent years (Bastia, 2006; Collett et al. 2008) attract the scientific community to study the basin in greater detail. The basin has significant hydrocarbon potential both in the Tertiary delta as well as in the channel-levee-over bank play types in the deepwater region. Major delta systems with thick argillaceous and arenaceous facies have prograded basin ward after the rifting of the basin during the Late Cretaceous. Large canyons of different magnitude have also contributed to the total sediment accumulations. The fast rate of deposition on the slope-intraslope basins has led to the development of fault extensions (Bastia, 2006).

The basin evolved through rifting and subsequent drifting during the Mesozoic. The Mesozoic and subsequent Early Tertiary deep water sequence provide the base for the Late Tertiary marine sediments brought in by either large canyon systems or feeder channels in the upper slope. Several V-shaped canyons flanked by steep faults characterize the upper to middle slope regions, while turbidity channels and levee wedges traverse the shelf and slope (Prasad and Rangaraju, 1987). Sediment input in this region has been dominated by the Krishna and Godavari river systems. The KG Basin is orthogonally juxtaposed to NW-SE trending Pranhita Godavari Gondwana graben in the north. The NE-SW basin margin is the most extensive fault trend near

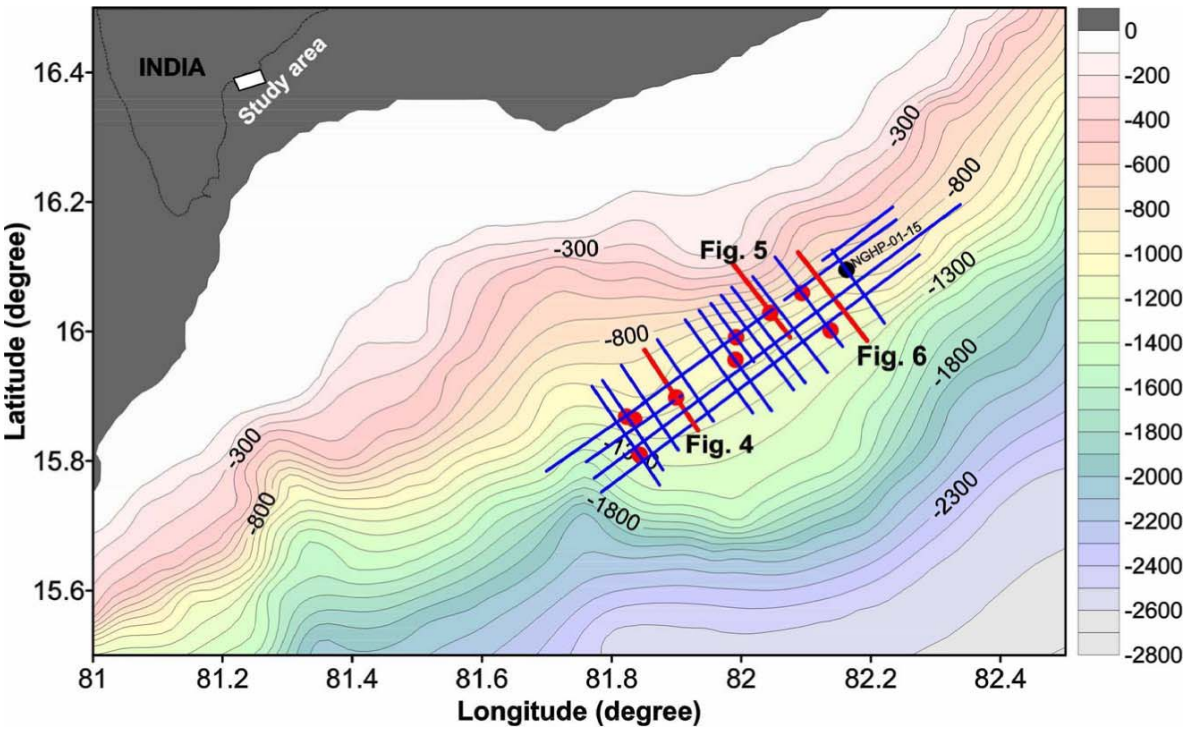

Fig.1. Bathymetry map of the Krishna-Godavari (KG) basin, off the eastern Indian margin. Location of drill sites by the NGHP-01 are shown with red circles. Solid blue lines are the 2D high resolution MCS lines. Bold red lines with corresponding figure numbers represent the lines used in this study. The color bar represents the water depth in meter below sea surface. Contours are also shown to indicate water depth directly. Inset shows location of the KG Basin on the east coast off India.

Kakinada graben in the northeast and near Palar-Pennar graben in the southwest (Gupta, 2006). The high rate (~20-25 cm/ky) of sedimentation (Rao et al. 1994) and total organic carbon content (TOC) of 1.5–2.0% (Kundu et al. 2008) show favorable conditions for significant methane generation in the KG Basin.

MATERIALS AND METHODS

Heat Flow Derived from BGHSZ

Since, the BSR closely approximates the base of gas hydrate stability zone, the BSR depths can be used to derive the local variations in heat flow due to tectonic disturbances and fluid flow through faults acting as migration pathways (Yamano et al. 1982; Townend, 1997; Ganguly et al. 2000; Kaul et al. 2000; Vohat et al. 2003; Shankar and Sain, 2009; Horozal et al. 2009). This was done by assuming a linear temperature gradient and following simple conductive heat transport relationship:

$$HF = 1000 \times k \times \left(\frac{T_{BGHSZ} - T_{sf}}{\Delta D} \right) \quad (1)$$

Where, HF is the heat flow in mW/m^2, k is the thermal conductivity in W/mK, T_{BGHSZ} and T_{sf} are the temperatures at the BGHSZ and seafloor respectively in °C. ΔD (in m) is the distance from the seafloor to the predicted depth of the BGHSZ.

The T_{sf} is estimated using the linear regression from in situ temperature measurements by the NGHP-01 which is comparable with the CTD measurements by Mazumdar et al. (2007): T_{sf} =13.09-0.0062×z, where z is water depth in meter. The T_{BGHSZ} is estimated using the experimental thermobaric stability condition for the methane–seawater system (Bouriak et al. 2000), which is based on pure methane and standard seawater (34 ppt). The thermal conductivity (k) is a function of depth below the seafloor, and is taken from the NGHP-01 at all sites cored in the KG area (Collett et al. 2008). The ΔD is determined from velocity function deduced from the sonic logs (Collett et al. 2008; Shankar et al. 2010). We further assumed a hydrostatic pressure regime and calculated the pressure using a constant water density of 1030 kg/m^3.

Estimation of Gas Hydrate Saturation

Pure gas hydrate has much higher velocity than that of oceanic sediment in which it occurs. Thus the most readily observable physical change for hydrate-bearing sediment is an increase in seismic velocity, which is proportional to gas hydrate concentration (Pearson et al. 1983). Gas hydrate-bearing sediments are also characterized by high resistivity anomalies. If we assume that the resistivity anomalies are caused by gas hydrate present in pore spaces of sediments, then the gas hydrate saturation S_h is given by Archie's equation (1942):

$$R_o = \left(aR_w \Big/ \varphi^m \right) \quad (2)$$

Where, R_o is the formation resistivity of water-saturated sediment, R_w is the resistivity of the pore water, φ is the porosity, a and m are the Archie constants, known as the Archie coefficient and cementation factor respectively. R_w is predicted by a linear least-square regression fit with depth of in situ pore water resistivity data derived from the salinity measurement during the NGHP-01, and the regression equation is given as

$$R_w = 0.2843 - 0.0002 \text{ x } z \quad (3)$$

Where, z is the depth below seafloor in meters. The regression is quite robust with a value of more than 90% (solid line in Fig. 2). After predicting R_w, we estimate $R_{0,}$ which is used as the background resistivity for this site. The a and m values depend on the interaction between the host sediments and gas hydrate in the porous medium. Equation (2) can be solved for the ratio of water saturated sediment resistivity and the connate water resistivity, which gives formation factor (i.e. $F = R_o / R_w = a\varphi^{-m}$). The gas hydrate saturation (S_h) in the formation from the resistivity log data can be estimated now from the Archie equation as

$$S_h = 1 - \left(aR_w \varphi^{-m} \Big/ R_t \right)^{1/n} \quad (4)$$

RESULTS AND DISCUSSION

Phase Boundary and GHSZ at Site 15 of the NGHP-01

The GHSZ thickness is determined by water depth, pore pressure, seafloor temperature, thermal gradient, and gas and fluid composition. Using the BSR as the BGHSZ, we determine the potential gas hydrate stability thickness at site 15 of the NGHP-01, which is 126 meter below seafloor (mbsf) (Fig. 3). Simultaneously, we model the phase diagram using the depths of seafloor and BSR, water temperature profile and geothermal gradient observed during the NGHP-01 using the Brown et al. (1996) and the Sloan (1998) approaches, which is based on an empirical algorithm for the stability of methane hydrate in seawater with a variable salinity. The Brown et al. (1996) (red line) phase diagram is

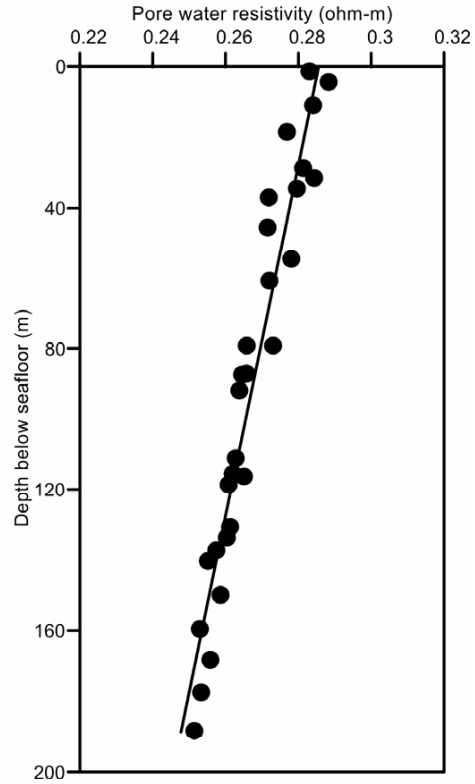

Fig.2. Calculated resistivity of connate water (R_w) at site 15 of the NGHP-01 with measured temperature and salinity from Fofonoff (1985) equation of state for sea water. Solid line shows the best linear fit, and making this linear regression equation, water saturated resistivity has been estimated.

in good agreement with the Sloan (1998) (dotted blue line) phase diagram (Fig. 3). As the water depth increases, the temperature threshold for gas hydrate also increases. At a given water depth, the temperature thresholds for Sloan (1998) is little bit more than that of Brown et al (1996). Knowing the water depth and thermal gradient at a particular location, the GHSZ can be estimated by finding the seafloor temperature (black curve in Fig. 3) and drawing a straight line to the appropriate thermal gradient. The depth at which the thermal gradient line intersects the gas hydrate phase curve represents the lower boundary of gas hydrate stability zone. It is to be mentioned here that the temperature required for gas hydrate destabilization is higher when additional higher hydrocarbons are present in the gas phase, while a higher salinity has the opposite effect (Claypool and Kvenvolden, 1983; Dickens and Quinby-Hunt, 1994; Brown et al. 1996).

The BSR depth predicted from this phase diagram matches reasonably well with the depth of BSR observed on seismic section. However, small differences in phase boundary temperature are observed at grater depths due to fluid composition (Dickens and Quinby-Hunt, 1994). The

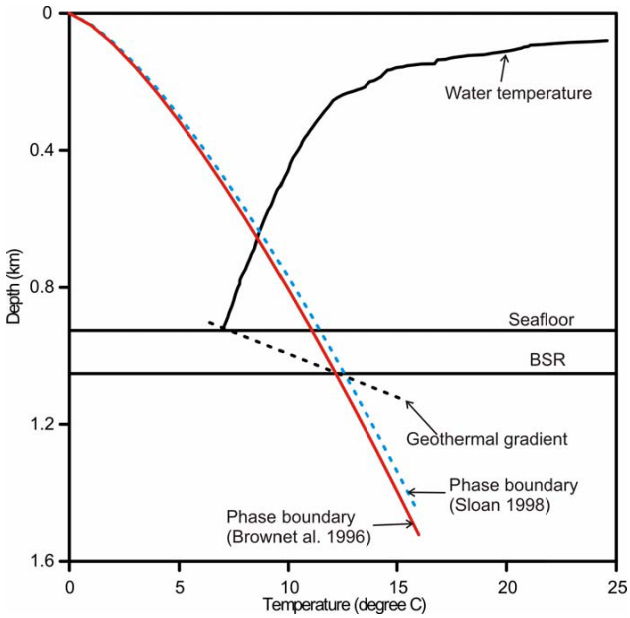

Fig. 3. Methane hydrates stability curve of Brown et al. (1996) and Sloan (1998) for site 15 of NGHP-01 in the KG basin. Geothermal gradient interpolated from the in situ temperature measurements. Water temperature profile of CTD measurements is taken from Mazumdar et al. (2007).

seafloor temperature, measured in situ at site 15 and fitted to water temperature CTD measurements (Mazumdar et al. 2007) is utilized in this study. The depths of seafloor and BSR are marked on the stack section in Fig.3. Geothermal gradient for the upper sedimentary layer is calculated from the in situ measurement and its linear extrapolation, shown with black dash line in Fig.3.

Forward Modeling of the BGHSZ

In order to map the distribution of BGHSZ, and to understand the changes in BSR occurrences, and amplitude characters across the 2D seismic profiles, we use 1D thermal modeling to predict the BGHSZ as described by Shankar et al. (2010). We assume a hydrostatic pressure regime, uniform thermal conductivity (based on little variation observed during the measurements of NGHP-01), and a uniform P-wave velocity structure with a gradual increase from seafloor to BSR. We use the gas hydrate (structure I) stability curve calculation by Bouriak et al. (2000), based on pure methane and on average standard seawater salinity (34 ppt), which is in good agreement with the geochemical pore-water and void gas measurements made at various sites of NGHP-01. The seafloor temperatures and thermal gradients are allowed to change according to water depth variation across the 2D data using the database of thermal measurements established during the NGHP-01.

The geothermal modeling is performed to predict the

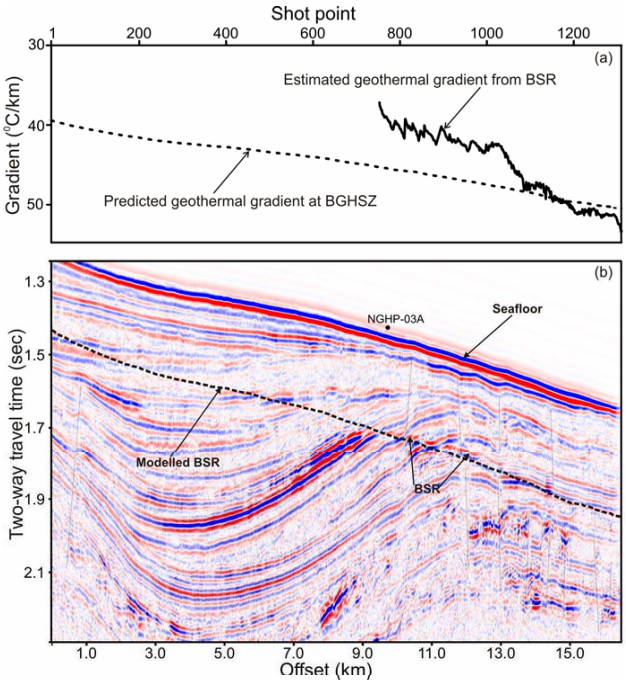

Fig. 4: **(a)** Estimated geothermal gradient (shown with solid curve) from the position of the BSR and the predicted geothermal gradient (dotted curve) at BGHSZ. **(b)** 2D MCS profile crossing the site 03A (shown by small black circle on seafloor) of NGHP-01. A BSR of moderate strength is observed along the profile with cross-cutting of dipping sedimentary reflectors. Modeled BGHSZ (or BSR) is shown with dotted black line. Please see Fig.1 for location.

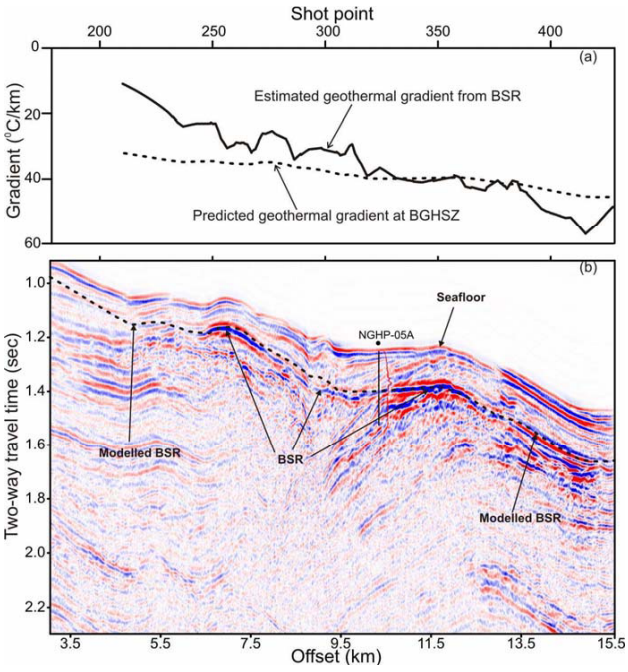

Fig. 5. (a) Estimated geothermal gradient (shown with solid curve) from the position of the BSR and the predicted geothermal gradient (dotted curve) at BGHSZ. **(b)** 2D MCS profile crossing the site 05A (shown by small black circle on seafloor) of NGHP-01. A BSR of moderate to high amplitudes is observed along the profile. Modeled BGHSZ (or BSR) is shown with dotted black line. Please see Fig.1 for location.

theoretical BGHSZ. Overall, the modeled BGHSZ (black dotted line on all seismic sections displayed in Figs. 4, 5 and 6) correspond well to the observed BSRs. The fluctuations of the predicted BGHSZ from the observed BSRs are likely due to errors arising from picking the seafloor, variability of seafloor temperature and geothermal gradient, which is function of water depth (Shankar et al. 2010).

Geothermal Gradient and Heat Flow

The geothermal gradient and heat flow is determined from the depth of BSRs identified on three seismic profiles (Figs. 4, 5 and 6). The heat flow values are similar to those obtained by Shankar and Riedel (2010). The geothermal gradients calculated directly from the depths of BSRs are shown by black curves and the predicted geothermal gradients at BGHSZ are shown with dotted curves (Figs. 4a, 5a and 6a). We observe that there is no focused fluid flow and abnormal geothermal trend in the study area. However, we notice faults in deeper parts (Fig. 4b) but not reaching to the seafloor.

The study shows that the estimated and the predicted geothermal gradients at BGHSZ increase towards deeper water. As a whole, the average geothermal gradient in the study area is ~40°C/km. There are pronounced difference in predicted and estimated geothermal gradient, which is likely due to the variability of calculated seafloor and BSR temperature that are sensitive to change in seafloor topography. The main changes are due to errors in picking the BSR and seafloor.

In marine gas hydrate areas, the heat flow can be estimated from the depth of the BSR, which is generally very close to the BGHSZ (e.g. Yamano et al. 1982; Davis et al. 1990; Ganguly et al. 2000; He et al. 2007). Alternatively, where a BSR can not be seen, the BGHSZ can be predicted if seafloor temperature and geothermal gradient are known. BSRs in the KG Basin are well imaged on the continental slope and are very weak or absent in the basin plain (Collett et al. 2008; Ramana et al. 2009). Regional heat flow calculated from the depth of the BSR identified on seismic dataset from the KG Basin. The estimated heat flow ranges from 23 to 62 mW/m^2 (Fig. 7). The heat flow distribution closely correlates with the bathymetry. Higher heat flow occurs in the deeper southern part of the study area and

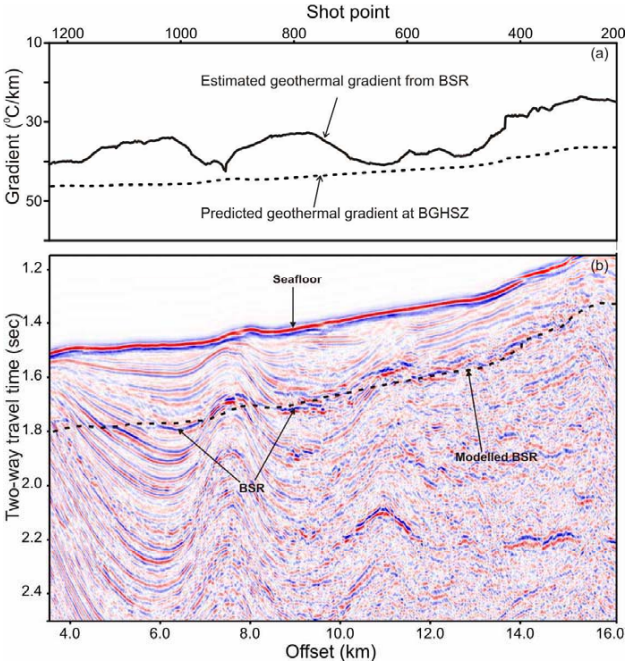

Fig. 6. (a) Estimated geothermal gradient (shown with solid curve) from the position of the BSR and the predicted geothermal gradient (dotted curve) at BGHSZ. **(b)** 2D MCS profile with low amplitude BSR is observed. Modeled BGHSZ (or BSR) is shown with dotted black line. Please see Fig.1 for location.

lower heat flow is observed in the shallower northeastern part of the study area at water depths less than 1000 m, where there has been little recent extension. These values are similar to those derived from modeling of the high resolution of the bathymetry data, ranging from 30 to 102 mW/m^2 (Shankar and Riedel, 2010).

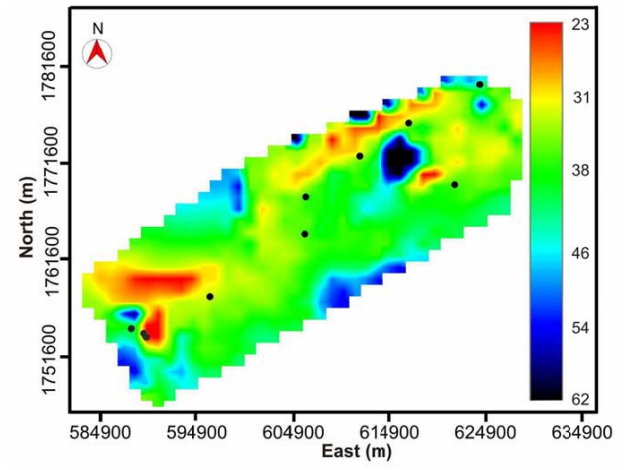

Fig.7. Regional heat flow map derived from the geothermal modeling of BSR as constrained by 2D seismic profiles. The color bar represents the heat flow values in mW/m^2.

Determination of Archie Parameters

For quantification of gas hydrate using the electrical resistivity log data, we apply the Archie relationship to the resistivity and porosity logs recorded at sites 15 in the KG Basin. By using the Archie's (1942) law, sediment bulk electrical resistivity for purely (saline) water-saturated sediments can be calculated using equation 2. We calculate R_w using the equation of state of seawater (Fofonoff, 1985). Assuming the pressure to be hydrostatic, in situ temperature measurements, core salinity measurements, and the geothermal gradient constrained from the NGHP-01 are utilized to derive the resistivity of connate water. Figure 2 shows the pore-water resistivity versus depth (in mbsf) profiles derived from the core-salinity, seafloor temperature, and geothermal gradient for site 15. Solid lines represent the smooth linear fit for the interpolation of the R_w using linear fit regression equation 3. The calculated R_w from the measured salinity and temperature along with estimated electrical resistivity shows slightly decrease in resistivity with depth below the seafloor. We utilize density-porosity relation in our calculation. Empirical Archie parameters a and m can then be estimated from a cross-plot of formation factor (F) and density porosity (φ) data with exponential fit for sediments containing no gas hydrate (Fig.8).

Figure 9a shows the difference between the calculated in situ resistivity (R_o) and measured log-resistivity (R_t), and demonstrates that the calculated R_o agrees well with the

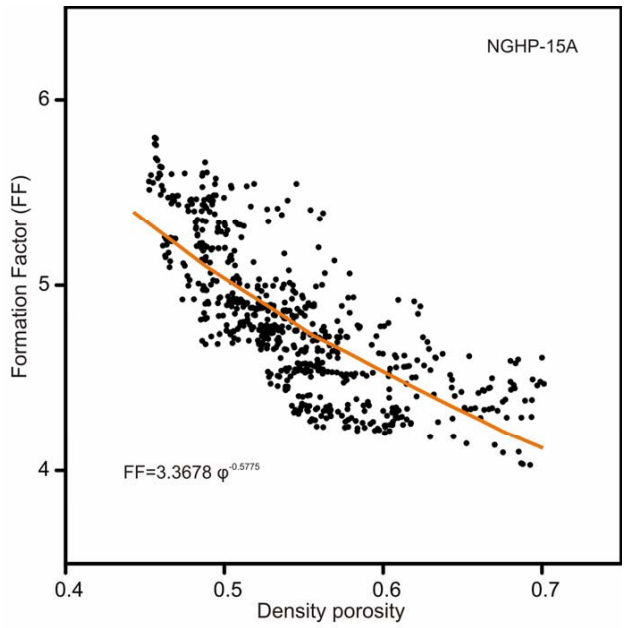

Fig.8. Formation factor versus porosity is plotted at site 15 of NGHP-01. The orange solid line is the best exponential fit, giving the Archie's parameters.

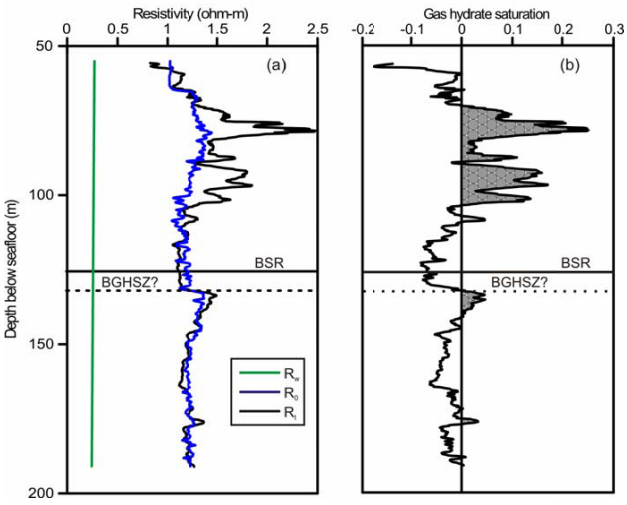

Fig.9. (a) Pore water resistivity R_w (green), measured LWD resistivity R_t (black) and 100% water-saturated resistivity R_o (blue), determined from the Archie analysis of downhole data at site 15 of NGHP-01. R_o is calculated from the log density porosity. **(b)** Gas hydrate saturation estimated from resistivity log data using the Archie analysis for the site 15 of NGHP-01 calculated using the log density porosity method.

measured resistivity for most intervals; however the calculated R_o is higher than the measured resistivity where significant amount of shale (clay) exists. This implies that the clay-effect on resistivity may be significant, partly because of the high resistivity of the connate water itself.

Gas Hydrate Saturation (S_h) Estimation from Resistivity Log

There is an extensive literature on the use of well logs for the estimation of gas hydrates (Collett, 2001; Kleinberg et al. 2005; Lee and Collett, 2008; Mathews, 1986; Guerin et al. 1999; Hyndman et al. 1999; Ghosh et al. 2010a, b). The most commonly used logs for the estimation of gas hydrate include the sonic and resistivity logs. Empirically estimated Archie parameters *a, m,* and *n* can be used to calculate S_h using equation 4. It is to be noted that the estimation of gas hydrate saturation from the electrical resistivity log data is sensitive to *n* value at higher gas hydrate saturations. From a physical perspective, choosing a value for *n* similar to that of *m* implies the assumption that the effect of gas hydrate formation on the electrical resistivity is similar to that of simple effective porosity reduction. Pearson et al., (1983) calculated n as 1.94. According to Spangenberg (2001), n depends somewhat on grain size distribution and the gas hydrate saturation itself. Here we use $n = 1.94$ for our calculations.

Down-hole profile of gas hydrate saturation (S_h) from resistivity at site 15 is shown in Fig.9b. This brings out two zones with high gas hydrate saturations: (i) up to 20-25% in the interval between 70 and 82 mbsf and (ii) less than 20% in the interval between 90 and 104 mbsf.

CONCLUSIONS

High resolution 2D MCS data in the KG basin shows widespread occurrences of BSRs and hence gas hydrates. The structural elements like the faults or fractures and seafloor morphology are important, which control the distribution of BSRs. The BSR-derived heat flows (23–62 mW/m^2) are quite favourable to the formation of gas hydrate in the KG Basin. Over all, the heat flow trends follow the seafloor bathymetry of the basin and systematic increase of heat flow is observed except local variations at few places. The BSR-derived heat flow across the major topographic features corresponds well with the expected trend (low heat flow values at high topography and vice versa) due to focusing and defocusing effect of the topography. There are currently no probe measurements available from the study area, however in situ geothermal gradient measurements from NGHP-01 are comparable with the estimated values.

The thermal modeling of BGHSZ shows close correspondence between the observed and modeled BSR depths on seismic sections (Fig. 4b, 5b and 6b). This modeling approach is very useful for providing the continuity of the BGHSZ especially where a BSR does not exist or scanty or is disturbed by local tectonic activity, or masked by other sedimentation patterns parallel to seafloor.

Gas hydrate-bearing sediments have high acoustic impedance and these impedance anomalies are controlled primarily by the degree of gas hydrate saturation, which can be determined using Archie's equation. The maximum gas hydrate concentration at site 15 is estimated up to ~25% in the pore spaces of sediments. The results suggest that in the KG basin, gas hydrate saturation is high in the gas hydrate stability zone, but free gas is meager beneath this zone. It is the scarcity of free gas that has led to the low amplitudes of the BSRs.

Acknowledgements: We thank the Director, NGRI for his kind permission to publish this work. We would like to acknowledge DGH, ONGC and the scientists and crew-members of Expedition 01 Indian NGHP, who acquired the log and core data. We also like to thank the Ministry of Earth Sciences, Govt. of India, New Delhi for supporting the Gas-hydrate Project at NGRI. Uma Shankar is grateful to the Department of Science and Technology, Govt. of India, New Delhi for the BOYSCAST Fellowship, 2008–2009.

References

Andreassen, K. (1995) Seismic studies of a bottom simulating reflection related to gas hydrate beneath the continental margin of the Beaufort Sea. Jour. Geophys. Res., v.100(B7), pp.12659-12673.

Archie, G.E. (1942) The electrical resistivity log as an aid in determining some reservoir characteristics. Trans. Amer. *Instt.* Min. Metall. Engg., v.146, pp.54-62.

Bastia, R. (2006) An overview of Indian sedimentary basins with special focus on emerging east coast deepwater frontiers. The Leading Edge, v.25(7), pp.818-829.

Biksham, G. and Subrahmanyam, V. (1988) Sediment transport of the Godavari River Basin and its controlling factors. Jour. Hydrology, v.101, pp.275-90.

Bouriak, S., Vanneste, M. and Saoutkine, A. (2000) Inferred gas hydrates and clay diapirs near the Storegga Slide on the southern edge of the Voring Plateau, offshore Norway, Marine Geology v.163, pp.125–148.

Brown, K.M., Bangs, N.L., Froelich, P.N. and Kvenvolden, K.A. (1996) The nature, distribution and origin of gas hydrate in the Chile Triple region. Earth Planet Sci. Lett., v.139, pp.471-483.

Claypool, G.E. and Kvenvolden, K.A. (1983) Methane and other hydrocarbon gases in marine sediment. Annual Rev. Earth Planet. Sci., v.11, pp.299-327.

Cooper, A.K. and Hart, P.E. (2003) High-resolution seismic-reflection investigation of the northern Gulf of Mexico gas hydrate stability zone. Marine Petrol. Geol., v.19, pp.1275-1293.

Collett, T.S. (2001) A review of well-log analysis techniques used to assess gas-hydrate-bearing reservoirs. *In:* C.K. Paull and W.P. Dillon (Eds.), Natural Gas Hydrates: Occurrence, Distribution, and Detection, Geophysical Monographs, v.124, pp.189-210.

Collett, T.S. (2002) Energy Resource Potential of Natural Gas Hydrates. Amer. Assoc. Petrol. Geol. Bull., v.86(11), pp.1971-1992.

Collett, T.S., Riedel, M., Cochran, J.R., Boswell, R., Presley, J., Kumar, P., Sathe, A.V., Sethi, A., Lall, M., Sibal, V. and NGHP Expedition 01 Scientists (2008) National Gas Hydrate Program Expedition 01 initial reports, Directorate General of Hydrocarbons, New Delhi.

Curray, J.R., Emmel, F.J., Moore, D.G. and Raitt, R.W. (1982) Structure, tectonics and geological history of the Northeastern Indian Ocean. *In:* A.E. Nairn and F.G. Stehli (Eds.), The ocean basins and margins, v.6, Plenum, New York, pp.399-450.

Curray, J.R. (1991) Possible greenschist metamorphism at the base of a 22-km sedimentary section, Bay of Bengal. Geol., v.19, pp.1097-1100.

Davis, E.E., Hyndman, R.D. and Villinger, H. (1990) Rates of fluid expulsion across the northern Cascadia accretionary prism: constraints from new heat flow and multichannel seismic reflection data. Jour. Geophys. Res., v.95, pp.8869-8889.

Dickens, G.R. and Quinby-Hunt, M.S. (1994) Methane hydrate stability in seawater. Geophys. Res. Lett., v.21(19), pp.2115-2118.

Federov, L.V., Ravich, M.G. and Hofmann, J. (1982) Geologic comparison of southeastern peninsular India and Sri Lanka with a part of Antarctica. *In:* C. Craddock (Ed.), Antarctic Geology and Geophysics. University of Wisconsin Press, Madison, Wisconsin, USA, pp.157-171,

Fichler, C., Henriksen, S., Rueslaatten, H. and Hovland, M. (2005) North Sea Quaternary morphology from seismic and magnetic data: indications for gas hydrates during glaciations. Petroleum Geoscience, v.11, pp.331-337.

Fofonoff, N.P. (1985) Physical properties of seawater: a new salinity scale and equation of state for seawater. Jour. Geophys. Res., v.90(C2), pp.3332-3342.

Ganguly, N., Spence, G.D., Chapman, N.R. and Hyndman, R.D. (2000) Heat flow variations from bottom simulating reflectors on the Cascadia margin. Marine Geol., v.164, pp.53-68.

Ghosh, R., Sain, K. and Ojha, M. (2010A) Effective medium modeling of gas hydrate-filled fractures using sonic log in the Krishna-Godavari basin, eastern Indian offshore. Jour. Geophys. Res., v.115, B06101, pp.1-15.

Ghosh, R., Sain, K. and Ojha, M. (2010B) Estimating the amount of gas hydrate using effective medium theory: a case study in the Blake Ridge. Marine Geophys. Res., Spec. Issue no.31, pp.29-37.

Guerin, G., Goldberg, D. and Melsterl, A. (1999) Characterization of in situ elastic properties of gas hydrate-bearing sediments on the Blake Ridge. Jour. Geophys. Res., v.104, pp.17781-17796.

Gupta, S.K. (2006) Basin architecture and petroleum system of Krishna Godavari Basin, east coast of India, The Leading Edge, v.25(7), pp.830-837.

Helgerud, M.B., Dvorkin, J. and Nur, A. (1999) Elastic-wave velocity in marine sediments with gas hydrates: Effective medium modeling. Geophys. Res. Lett., v.26, pp.2021-2024.

He, T., Spence, G.D., Riedel, M., Hyndman, R.D. and Chapman, N.R. (2007) Fluid flow and origin of a carbonate mound offshore Vancouver Island: Seismic and heat flow constraints. Marine Geol., v.239, pp.83-98.

Holbrook, W.S., Hoskins, H., Wood, W.T., Stephen, R.A., Lizarralde, D. and Leg 164 Science Party (1996) Methane hydrate and free gas on the Blake Ridge from vertical seismic profiling. Science, v.273, pp.1840-1843.

Horozal, S., Lee, G.H., Yi, B.Y., Yoo, D.G., Park, K.P., Lee, H.Y., Kim, W., Kim, H.J. and Lee, K. (2009) Seismic indicators of gas hydrate and associated gas in the Ulleung Basin, East Sea (Japan Sea) and implications of heat flows derived from depths of the bottom-simulating reflector. Marine Geol., v.258, pp.126-138.

Hovland, M., Gardner, J.V. and Judd, A.G. (2002) The significance of pockmarks to understanding fluid flow processes and geohazards. Geofluids, v.2, pp.127-136.

Hyndman, R.D. and Spence, G.D. (1992) A seismic study of

methane hydrate marine bottom simulating reflectors. Jour. Geophys. Res., v.97(B5), pp.6683-6698.

Hyndman, R.D., Yuan, T. and Moran, K. (1999) The concentration of deep sea gas hydrates from downhole electrical resistivity logs and laboratory data. Earth Planet. Sci. Lett., v.172(1-2), pp.167-177.

Hyndman, R.D., Spence, G.D., Chapman, N.R., Riedel, M. and Edwards, R.N. (2001) Geophysical Studies of Marine Gas Hydrate in Northern Cascadia. *In:* C.K. Paull and W.P. Dillon (Eds.), Natural gas hydrates: occurrence, distribution, detection. Amer. Geophys. Union Monographs, v.124, pp.273-295.

Kaul, N., Rosenberger, A. and Villinger, H. (2000) Comparison of measured and BSR derived heat flow values, Makran accretionary prism, Pakistan. Marine Geol., v.164, pp.37-51.

Kleinberg, R.L., Flaum, C. and Collett, T.S. (2005) Magnetic resonance log of JAPEX/JNOC/ GSC et al. Mallik 5L-38 gas hydrate production research well: gas hydrate saturation, growth habit, relative permeability. *In:* S.R. Dallimore, and T.S. Collett (Eds.), Scientific Results from the Mallik 2000 Gas Hydrate Production Research Well Program. Geolog. Surv. Canada Bull., v.585, pp.10, Mackenzie Delta, Northwest Territories, Canada.

Kundu, N., Pal, N., Sinha, N. and Budhiraja, I.L. (2008) Paleo hydrate and its role in deep water Plio-Pleistocene gas reservoirs in Krishna-Godavari basin, India, Proceedings of 6th ICGH, Vancouver, British Columbia, Canada, July 6-10. https://circle.ubc.ca/bitstream/2429/1065/1/5567.pdf

Kvenvolden, K.A. (1998) A primer on geological occurrence of gas hydrate. *In:* J.P. Henriet and J. Mienert (Eds.), Gas Hydrates: Relevance to World Margin Stability and Climate Change. Geol. Soc. London Spec. Publ., v.137, pp.9-30.

Kvenvolden, K.A. (1999) Potential effects of gas hydrate on human welfare. Proc. National Acad. Sci., USA, v.96, pp.3420-3426.

Lee, M.W. and Collett, T.S. (2008) Integrated analysis of well logs and seismic data at the Keathley Canyon, Gulf of Mexico, for estimation of gas hydrate concentrations. Marine and Petroleum Geol., v.25, pp.924-931.

Lee, M.W. and Waite, W.F. (2008) Estimating pore-space gas hydrates saturations from well-log acoustic data, Geochemistry Geophysics Geosystems, v.9(7), Q07008, doi:10.1029/2008GC002081.

Mathews, M. (1986) Logging characteristics of methane hydrate, The Log Analyst, v.27(3), pp.26-63.

Mazumdar, A., Paropkari, A.L., Borole, D.V., Rao, B.R., Khadge, N.H., Karisiddaiah, M., Kocherala, M. and Hilda, M.J. (2007) Pore-water sulfate concentration profiles of sediment cores from Krishna-Godavari and Goa basins, India. Geochmical Jour., v.41, pp.259-269.

Minshull, T.A., Singh, S.C. and Westbrook, G.K. (1994) Seismic velocity structure at a gas hydrate reflector, offshore western Columbia, from full waveform inversion, Jour. Geophys. Res., v.99, pp.4715-4734.

Paull, C.K. and Dillon, W.P. (Eds.) (2001) Natural Gas Hydrate: Occurrence, Distribution and Detection. Amer. Geophys. Union Monograph Series, v.124, pp.53-66.

Pearson, C.F., Halleck, P.M., McGuire, P.L., Hermes, R. and Mathews, M. (1983) Natural gas hydrate: a review of in situ properties. Jour. Physical Chemistry, v.87, pp.4180-4185.

Powell, C.M., Roots, S.R. and Veevers, J.J. (1988) Pre-breakup continental extension in East Gondwanaland and the early opening of the eastern Indian Ocean. Tectonophysics, v.155, pp.261-183.

Prabhakar, K.N. and Zutshi, P.L. (1993) Evolution of southern part of Indian East Coast Basin. Jour. Geol. Soc. India, v.41, pp.215-230.

Prasad, K.L. and Rangaraju, M.K. (1987) Modern and recent canyon-fan systems in Masulipatnam Bay, Krishna–Godavari Basin, ONGC Bull., v.24(2), pp.59-71.

Ramana, M.V., Ramprasad, T. and Desa, M. (2001) Seafloor spreading magnetic anomalies in the Enderby Basin, East Antarctica. Earth Planet. Sci. Lett., v.191, pp.241-255.

Ramana, M.V., Ramprasad, T., Desa, M., Sathe, A.V. and Sethi, A.K. (2006) Gas hydrate-related proxies inferred from multidisciplinary investigations in the Indian offshore areas. Curr. Sci., v.91(2), pp.183-189.

Ramana, M.V., Ramprasad, T., Paropkari, A.L., Borole, D.V., Rao, B.R., Karisiddaiah, S.M., Desa, M., Kocherla, M., Joao, H.M., Lokabharati, P., Gonsalves, M.J., Pattan, J.N., Khadge, N.H., Babu, C.P., Sathe, A.V., Kumar, P. and Sethi, A.K. (2009) Multidisciplinary investigations exploring indicators of gas hydrate occurrence in the Krishna–Godavari Basin offshore, east coast of India. Geo-Marine Lett., v.29, pp.25-38.

Rao, D.P., Bhattacharya, G.C., Ramana, M.V., Subramanyam, V., Ramprasad, T., Krishna, K.S., Chaubey, A.K., Murty, G.P.S., Srinivas, K. and Desa, M. (1994) Analysis of multi-channel seismic reflection and magnetic data along 13^0 N latitude across the Bay of Bengal. Marine Geophys. Res., v.16, pp.225-236.

Rao, G.N. (2001) Sedimentation, stratigraphy, and petroleum potential of Krishna-Godavari basin, East coast of India. Amer. Assoc. Petrol. Geologists, v.85(9), pp.1623-1643.

Riedel, M., Novosel, I., Spence, G.D., Hyndman, R.D., Chapman, N.R. and Lewis, T. (2006) Geophysical and geochemical signatures associated with gas hydrate–related venting in the northern Cascadia margin. Geol. Soc. Amer. Bull., v.118(1), pp.23-38.

Riedel, M., Collett, T.S. and Shankar, U. (2010) Documenting channel features associated with gas hydrates in the Krishna-Godavari Basin, offshore India. Marine Geology, doi: 10.1016/j.margeo.2010.10.008.

Ruppel, C., Dickens, G.R., Castellini, D.G., Gilhooly, W. and Lizarralde, D. (2005) Heat and salt inhibition of gas hydrate formation in the northern Gulf of Mexico. Geophys. Res. Lett., v.32, pp.L04605.

Sager, W.W., Lee, C.S., MacDonald, I.R. and Schroeder, W.W. (1999) High-frequency near-bottom acoustic reflection signatures of hydrocarbon seeps on the northern Gulf of

Mexico continental slope. Geo-Marine Lett., v.18, pp.267-276.

Sain, K. and Gupta, H.K. (2008) Gas hydrates: Indian scenario. Jour. Geol. Soc. India, v.72, pp.299-311.

Sastri, V.V., Venkatachala, B.S. and Narayanan, V. (1981) The evolution of the east coast of India. Palaeogeo. Palaeont. Palaeoeco., v.36, pp.23-54.

Shankar, U. and Sain, K. (2009) Heat flow variation from bottom simulating reflector in the Kerala-Konkan basin of the western continental margin of India. Indian Jour.Marine Sci., v.38, pp.110-115.

Shankar, U., Riedel, M. and Sathe, A.V. (2010) Geothermal modeling of the gas hydrate stability zone along the Krishna Godavari Basin. Marine Geophys. Res., v.31, pp.17–28.

Shankar, U. and Riedel, M. (2010) Seismic and heat flow constraints from the Krishna-Godavari Basin gas hydrate system. Marine Geol., v.276, pp.1-13.

Shipley, T.H., Houston, M.H., Buffler, R.T., Shaub, F.J., McMillen, K.J., Ladd, J.W. and Worzel, J.L. (1979) Seismic reflection evidence for the widespread occurrence of possible gas-hydrate horizons on continental slopes and rises. Amer. Assoc. Petroleum Geol. Bull., v.63, pp.2204-2213.

Sloan, E.D. (1990) Clathrate Hydrates of Natural gases, Marcel Dekker, New York.

Sloan, E.D. (1998) Clathrate hydrates of natural gases, second edition Marcel Dekker Inc., New York, pp.628.

Spangenberg, E. (2001) Modeling of the influence of gas hydrate content on the electrical properties of porous sediments. Jour. Geophys. Res., v.106(B4), pp.6535–6548.

Townend, J. (1997) Estimates of conductive heat flow through bottom-simulating reflectors on the Hikurangi and southwest Fiordland continental margins, New Zealand. Marine Geol., v.141, pp.209-220.

Vohat, P., Sain, K. and Thakur, N.K. (2003) Heat flow and geothermal gradient from BSR: a case study. Curr. Sci., v.85, pp.1263-1266.

Yamano, M., Uyeda, S., Aoki, Y. and Shipley, T.H. (1982) Estimates of heat flow derived from gas hydrates. Geology, v.10, pp.339-343.

Yuan, T., Hyndman, R.D., Spence, G.D. and Desmons, B. (1996) Seismic velocity increase and deep-sea gas hydrate concentrations above a bottom-simulating reflector on the northern Cascadia continental slope. Jour. Geophys. Res., v.101, pp.13655-13671.

(Received: 23 February 2011; Revised form accepted: 30 June 2011)